A Green One-Pot Preparation Method for Very High Porous Solids Loading Paper Composites

*Pierre Tignol, Vanessa Pimenta, Anne-Laurence Dupont, Silvia Carvalho, Abeer Al Mohtar, Maria Inês Severino, Farid Nouar, Moisés L. Pinto, Christian Serre,*and Bertrand Lavédrine**

Pierre Tignol, Anne-Laurence Dupont, Bertrand Lavédrine
Centre de Recherche sur la Conservation, Muséum national d'Histoire naturelle, CNRS, Ministère de la Culture, 75005, Paris, France
E-mail: bertrand.lavedrine@mnhn.fr

Pierre Tignol, Vanessa Pimenta, Maria Inês Severino, Farid Nouar, Christian Serre
Institut des Matériaux Poreux de Paris, ESPCI Paris, Ecole Normale Supérieure, CNRS, PSL University, 75005, Paris, France
E-mail : christian.serre@espci.psl.eu

Silvia Carvalho, Abeer Al Mohtar, Moisés L. Pinto
CERENA, Departamento de Engenharia Química, Instituto Superior Técnico, Universidade de Lisboa, Campus Alameda, 1049-001 Lisboa, Portugal

Keywords: Metal Organic Frameworks, Cellulose, NFC, porous solids, paper sheet, adsorption.

Abstract

Owing to their high porosity and tunability, porous solids such as Metal-Organic Frameworks (MOFs), Zeolites and Activated Carbons (ACs) are of great interest in various fields for instance gas separation, catalysis, water and air purification, among others. These materials are usually in powder form and need to be shaped in some practical way that does not modify their intrinsic property (i.e. porosity). Making porous, freestanding and flexible sheets is a relevant shaping strategy. However, achieving high loadings (> 70 wt %) can challenge mechanical properties. We have developed a new green and simple method that combines two cellulosic fibrous structures of different size, i.e. softwood bleached kraft fibres (S) and nano-fibrillated cellulose (NFC), to form a high porous solids loading (>70 wt %) paper sheet. This dual fiber system produces a synergistic effect, where S provides flexibility while NFC acts as a nanostructuring and mechanical strengthening agent with an optimal S:NFC=25:75 ratio. This method can be applied for the preparation of sheets exhibiting the mechanical properties of paper while keeping the adsorption properties of a wide range of porous solids (MOFs, ACs, Zeolites). As an exemple of application, a MOF paper has been considered for the capture of polar volatile organic compounds, showing better performance than other shaping processes such as beads and granules.

1. Introduction

Porous solids are highly versatile materials due to their exceptional structural and chemical tunability. These characteristics allow them to interact specifically with a wide range of guest molecules (gases, vapours, liquids) making them appealing compounds of strong technological and scientific interest [1-3] in a wide range of applications such as catalysis [4], gas storage and separation [5,6], sensing [7], energy storage [8] and biotechnology [9].

In the past few decades, in addition to the continuous development of mature materials such as activated carbons, zeolites, clays, several new classes of porous solids have emerged among which Metal-Organic Frameworks (MOFs), Covalent-Organic-Frameworks (COFs), porous polymers and porous cages [10]. However, all these solids are often produced in powder form, thereby ruling out a number of practical applications. Shaping these solids is therefore a prerequisite insofar that this does not alter their intrinsic key property (e.g. porosity) [11,12]. Typical shaping methods consist in producing pellets, beads, monoliths and foams when associated with additives (solvent, binder) or specific process conditions (pressure, temperature), thereby requiring a case by case optimization for each porous solid to meet the requirements of the targeted application [13-15]. In addition, such treatments can lead to irreversible textural and structural changes for instance upon application of an excessive mechanical pressure [16], or alternatively to the release of powder if the mechanical stability is insufficient [17]. Binders, on the other hand, can lead to a partial pore blocking and/or to diffusion strong limitations [18].

Making fiber-based composites is a suitable shaping alternative to avoid these drawbacks [19]. They combine excellent mass transfer properties while holding a high porous solids content (>70 wt %), which ensures the highest possible efficiency in potential applications for gas adsorption [20], water purification [21], catalytic degradation [22] and biomedical applications [23]. Electrospinning is a simple, common technique which spins a blended porous solid/polymer suspension under a high voltage to form a stable, flexible and easy to handle freestanding composite [24]. Many synthetic polymers including polyacrylonitrile (PAN) [25], polystyrene (PS) [26], poly(vinylidene fluoride) (PVDF) [27] are generally used, leading to highly loaded porous solids composites (> 70 wt %) [28]. However, this method often results in a reduced specific surface area due to the encapsulation of the porous solid particles by the polymer and/or the use of hazardous solvents (DMF) that poison the pores of the adsorbent. As an alternative, other porous solid/fiber shaping strategies were developed such as solvent free hot-pressing [29,30] or textile fiber coating in aqueous/alcohol media [31]. However, this is

limited to a given category of porous solids (MOFs), and lower porous solids loadings (< 30 wt %) are typically obtained, which calls for the development of new methods to prepare environmentally-friendly fiber-based composites that may be easily scalable. In that respect, we have considered cellulose-based polymeric binders as an alternative that fulfills all the criteria to form a paper sheet composite with high loading of porous solids with superior performance.

Cellulose is the most abundant, natural and renewable biopolymer on earth with an annual biomass production of 1.5 x 10^{12} tons [32]. Wood, cotton seed and bast fiber pulps are biodegradable, affordable products and remain the main source of raw materials for the processing of cellulose. Cellulosic fibers used for papermaking have been combined with porous solids to produce filter papers with a high specific surface area for air purification [33]. In addition, due to its hydrophilic nature and chemical inertness, cellulose is of interest for wastewater purification while its biocompatibility is appealing for biomedical applications [34]. Due to the high degree of flexibility of plant fibers, porous cellulosic composites can also be integrated into electrochemical storage systems and conversion devices [35]. Cellulosic porous solids composites can be prepared following two main routes: (1) *in-situ* synthesis of porous particles in the presence of fibers and (2) *ex-situ* blending where particles are mixed with the fibrous material. Some attempts have been recently reported with the direct growth of zeolites or MOFs on plant fibers [36-38]. For instance, $Cu_3(BTC)_2$ (BTC=1,3,5-benzenetricarboxylate) [36] and γ-cyclodextrin-MOF [37] have been synthetized *in-situ* in the presence of plant fibers reaching a MOF content of about 6-15 wt % and 15-23 wt %, respectively, while zeolite A particles (30-40 wt %) have been deposited on plant fibers through a similar route [38]. However, only a low content of porous solids could be incorporated into the cellulosic substrate (5 to 40 wt %) without hampering the mechanical stability of the composite due to the disruption of the fiber network at higher filler content [39]. The strength of a paper depends not only on the fibers but also strongly on inter-fiber interactions. The fillers content is usually kept ca. 20-35 wt % to avoid a network per unit volume too low in fibers content, which ultimately reduces the strength of the paper [40]. Obtaining good mechanical stability at high particle loading (>70wt%) is therefore very challenging in terms of mechanical properties of the resulting composite paper sheet. The use of nanocellulose was proposed to achieve the desired properties. Nano-fibrillated cellulose (NFC), also denoted cellulose nanofibers (CNFs), possesses a nanostructure with a high aspect ratio (nanometers wide and up to several micrometers long) [41]. It can be extracted from cellulose fibers by mechanical and/or chemical treatment and produced industrially at the tons per day scale [42]. It offers the possibility to form strong, as

well as, complex fibers networks, with high tensile stiffness and strength [43,44]. Activated carbon (AC) papers with a loading of 50-90 wt %, prepared by *ex-situ* blending with NFC, showed good mechanical properties (high tensile strength *i.e.* 1.2 MPa for an AC paper sheet with a loading of 70 wt %) [45]. However, the formulation process includes multiple heating steps, while the flexibility of the composite as well as its sorption properties were not demonstrated. Several composites have also been reported based on 2,2,6,6-Tetramethylpiperidine-1-oxyl (TEMPO) oxidized cellulose nanofibers (TOCNF) with high density of carboxyl groups at the surface [46-48]. Few examples of *in-situ* synthesis and *ex-situ* blending in aqueous media have been associated with high loading of porous solids (>70 wt %) [49,50]. For instance, the *in-situ* synthesis route was applied to grow ZIF-8, UiO-66(Zr) and MIL-53(Al) nanoparticles on TOCNF with a loading of 75-90 wt % [49]. Zeolite (ZSM-5, silicalite-1 or Y) particles were alternatively mixed with TOCNF and polyethylene glycol (PEG) by *ex-situ* blending with a zeolite loading 60-97 wt %, resulting in composites with high flexibility [50]. However, these procedures, although associated in most cases with high loadings and good mechanical properties, still suffer from significant drawbacks such as partial pore blockade, multiple and/or lengthy (days) formulation steps at the cost of high energy-demanding hydro- or solvo-thermal conditions. These downsides make these processes not environmentally-friendly and rule out their practical use at large scale. Therefore, to the best of our knowledge, no green and economically viable procedure (Table S1) has been reported so far to produce high loading porous solids cellulosic based composites, while ensuring adequate sorption and mechanical properties.

NFC has also previously been used as a reinforcing agent to produce composites, for instance to prepare biomimetic amylopectin foams by freeze-drying [51] or mixed with acrylic resin to prepare an optical transparent polymer nanocomposite [52] leading in both cases to enhanced mechanical properties. In the case of cellulose based composites, NFC has also been used to increase mechanical strength properties of paper by improving the fibers interactions [53,54].

In this work, we report a versatile and sustainable one-pot method that consists in combining two cellulosic materials with different dimensions and aspect ratio, to prepare high porous solids loading (> 70 wt %) paper sheets with preserved adsorption properties and good mechanical stability. Softwood bleached kraft pulp fibers (SBKP abbreviated S further on) and NFC were selected to provide flexibility and tensile strength, respectively, resulting into a nanostructured paper-like mesh with enhanced content and retention of the porous solid particles. This low-energy, non-toxic, and straightforward process involves a rapid mixture, at room temperature in water, of the fibrous materials and the porous particles, followed by a rapid

filtering and drying step (**Figure 1**). To establish the proof of concept for the preparation of robust high porous solids loading paper sheets, we considered several parameters such as the porous solid loading, the particle size of the porous solid, the S to NFC ratio, and the pH of the suspensions to optimize the quality of the sheet as well as to shed light on the interaction mechanisms at play. The structure of the sheet was assessed through an analytical methodology combining characterization techniques such as powder X-Ray diffraction (PXRD), IR spectroscopy, thermal gravimetric analysis (TGA), nitrogen porosimetry, optical microscopy (OM), scanning electron microscopy (SEM) and 3D X-Ray microscopy. The mechanical properties were assessed using coaxial tensile strength and bending tests measurements. This easily scalable route was first optimized with a benchmark porous Metal-Organic Framework (MOF), the mesoporous Fe(III) trimesate MOF denoted MIL-100(Fe) (MIL stands for Materials of the Institute Lavoisier) prior to be extended to other MOFs as well as to a commercial zeolite and an activated carbon. Finally, as a first demonstration of the use of a MOF paper sheet, we considered a 75 wt % loaded MIL-100(Fe) paper for the capture of traces of a polar volatile organic compound, e.g. acetic acid, in heritage institutions to protect the artefacts. It showed that the MOF paper sheet exhibited equal performance to that of the MIL-100(Fe) powder while significantly outperforming the traditional shaped products such as beads or granules containing 85 - 95 wt % of MOF.

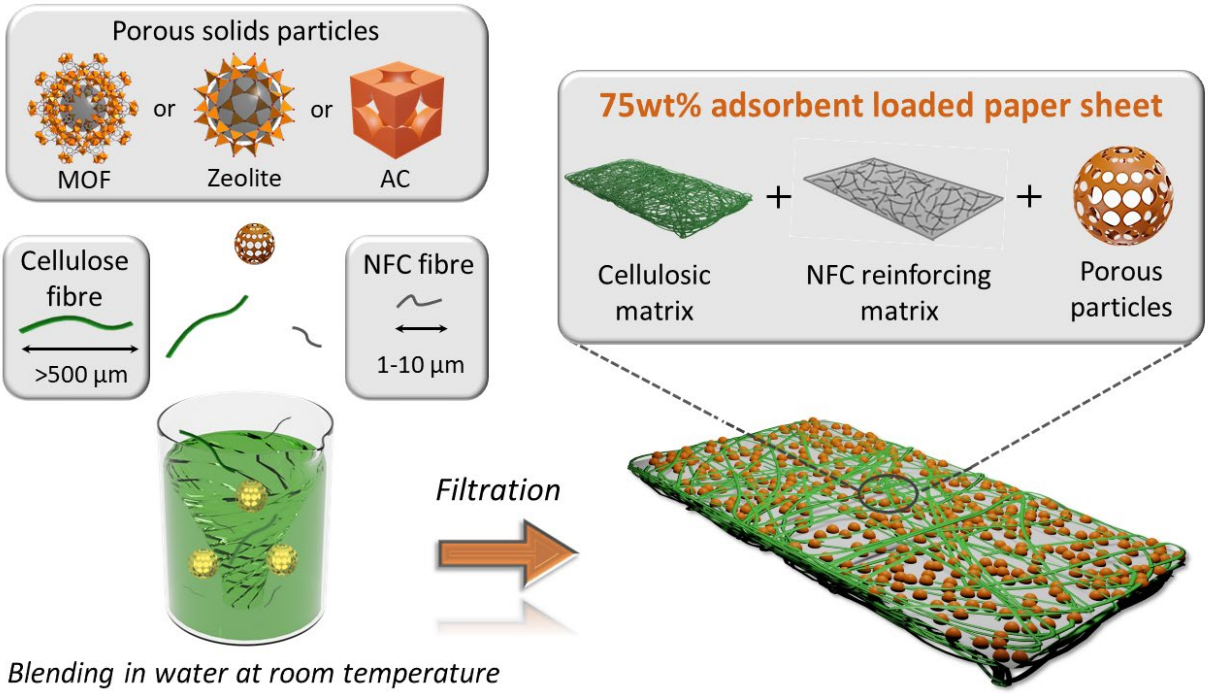

Figure 1. Scheme illustrating the green preparation process of the sheet containing different porous solids (Activated Carbon (AC), Metal-Organic Framework (MOF), Zeolite) combined with an NFC reinforced cellulosic matrix.

2. Results and discussion

2.1. The composite paper sheet

A paper sheet was prepared with 75 wt % MIL-100(Fe) embedded in a cellulose matrix composed of softwood fibres (S) and nano-fibrillated cellulose (NFC) (more details are given in the experimental section). MIL-100(Fe) that exhibits mesoporous cages (25 and 29 Å) accessible through microporous windows (5,7 and 8,2 Å) [55] was selected for the paper sheet optimization due to : (1) its biocompatibility, green and scalable synthesis [56,57] and (2) its physico-chemical properties (mesoporosity, hydrolytic stability, Lewis acid or redox active sites) of interest for a wide range of possible applications such as thermo-chemical energy [58,59], water purification [60,61], catalysis [62,63], gas storage [64,65] and biomedicine [66,67], among others. To reach the ambitious target of a 75 wt % loading of MIL-100(Fe) in a paper sheet with sufficient mechanical stability, we also considered using two distinct particle sizes for MIL-100(Fe) : microparticles (1 to 2 microns, Figure S1), denoted 'microMOF', prepared through a low temperature route (adapted from [68]), and nanoparticles (60 nm and few hundred nanometers as aggregates, Figure S2), denoted 'nanoMOF' prepared through a simple ambient pressure green route as reported previously (further details provide in the experimental section) [57,69].

Figure 2.a shows a paper sheet made of a mixture of S and NFC (25:75 ratio), and containing 75 wt % of microMOF. This sheet is ca. 20 cm in diameter, maximum size allowed by the fabrication mode (hand-sheet former machine). Note that the sheet could easily be made larger or smaller, in agreement with its simple and scalable preparation route. It is also significantly flexible (**Figure 2**.b). SEM images analysis indicates that the components are homogeneously distributed as shown on a cross-section that exhibits a dense packing structure with a thickness of about 400 µm (**Figure 2**.c). The PXRD pattern of the composite is also in good agreement with the one of MIL-100(Fe), simulated and experimental (**Figure 2**.d), indicating that the ambient conditions formulation process does not decrease the crystallinity of the MOF. The Fourier transform infrared (FTIR) spectra (**Figure 2**.e, S3) further confirm that the microMOF and the corresponding paper sheet exhibit similar main characteristic asymmetric and symmetric stretching bands: carboxylate groups at 1630-1577 cm^{-1} and 1448-1379 cm^{-1} (**Figure 2**.e) as well as trimeric Fe_3O sub-unit at 620 cm^{-1} (Fe-O bond) [68]. The slight differences between the powder and the composite lies in the 900 and 1200 cm^{-1} regions where cellulose bands are found: at 1160 cm^{-1} this corresponds to the asymmetric C-O-C vibration while those at 1031 and 1053 cm^{-1} are attributed to the C-C bond of the pyranose ring (**Figure 2**.f) [70].

Thermogravimetric analyses under oxygen atmosphere were first conducted on microMOF (**Figure 2.**g), S and NFC separately (Figure S4). The microMOF shows three weight losses corresponding to: (1) desorption of free solvent molecules from the pores (T < 100 °C), (2) removal of bound water molecules (100-250 °C) and (3) decomposition of the ligand at higher temperature (300 °C) [71]. S and NFC both exhibit an initial weight loss (> 90 wt %) until 150-200 °C due to the loss of physisorbed water prior to the onset of thermal decomposition at ca. 280 °C. S degrades completely between 280 °C and 310 °C whereas NFC degrades between 280°C and 450 °C. This is attributed to their slightly different compositions since S contains less thermally stable substances such as hemicelluloses and few residual lignin [72], prior to their conversion mainly into CO_2, H_2O and CO molecules [73]. The microMOF based paper sheet (**Figure 2**.g) exhibits a thermal behavior similar to the one of the raw materials, being stable up to 280 °C. The major weight loss of the composite (59 wt %) combines the degradation of the fibers and the MOF ligand, ultimately forming iron oxide Fe_2O_3. In addition, TGA enabled to estimate the MIL-100(Fe) content to about 77 wt %. N_2 porosimetry at 77 K was conducted on the microMOF and the composite sheet (**Figure 2**.h). Micro-MIL-100(Fe) exhibits the typical isotherm characteristic of micro/mesoporous solids with a first steep uptake at low partial pressure resulting in micropores filling at $P/P_0 < 0.015$, followed by two additional uptakes occurring at $P/P_0 = 0.06$ and 0.12 due to the coexistence of two mesopore types [55]. The porosity of the composite leads to a BET specific surface area close to 1540 ± 13 $m^2.g^{-1}$ versus 1920 ± 22 $m^2.g^{-1}$ for the microMOF. This is consistent with the percentage of MOF introduced (~75 wt %) considering that S and NFC contribute with negligible surface area, and confirming that the porosity of the MOF is fully preserved once in the paper sheet. Pore size distribution (PSD) estimated by DFT calculation (**Figure 2**.i) present peaks at 11.9, 17.9 and 21.6 Å for microMOF, corroborating the presence of micro/mesopores, showing little differences for the paper sheet.

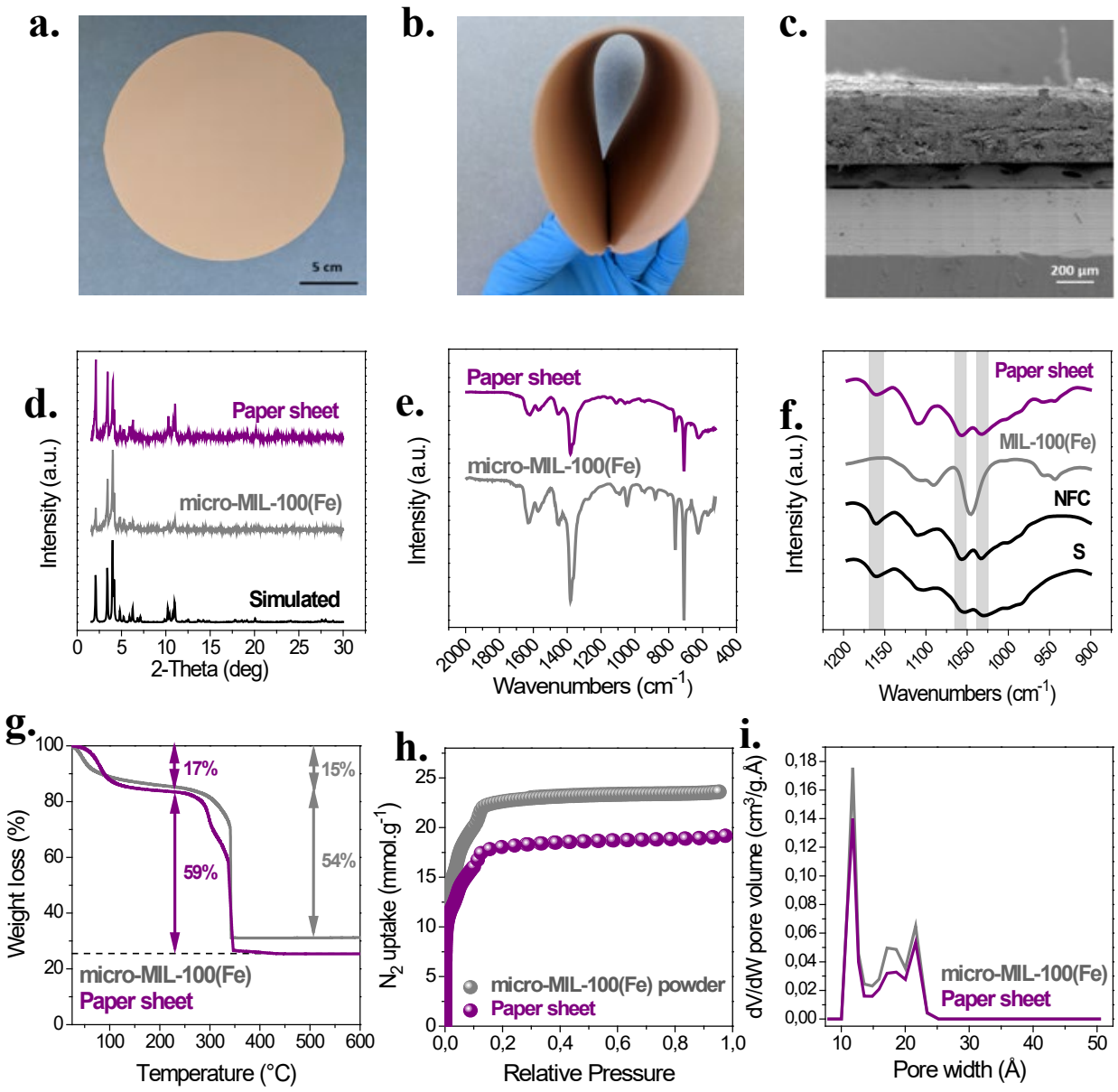

Figure 2. a) 75 wt % micro-MIL-100(Fe) paper sheet (cellulosic matrix = softwood bleached kraft pulp and NFC, ratio 25:75). b) Image showing the flexibility of the micro-MIL-100(Fe) paper sheet. c) SEM image of the cross-section of the sheet. d) PXRD patterns of simulated, micro-MIL-100(Fe) as powder and 75 wt % MIL-100(Fe) paper sheet (Cu-K_α, λ = 1,5406 Å). e) FTIR spectra of micro-MIL-100(Fe) as powder and in 75 wt % paper sheet in the range 500-2000 cm^{-1}. f) FTIR spectra of S, NFC, micro-MIL-100(Fe) as powder and in 75 wt % paper sheet in the range 900-1200 cm^{-1}. g) TGA of micro-MIL-100(Fe) and 75 wt % paper sheet. h) N_2 adsorption-desorption isotherms obtained at 77 K (adsorption, filled symbols; desorption, empty symbols) of micro-MIL-100(Fe) as powder and the corresponding paper sheet. i) Pore size distribution (PSD) of micro-MIL-100(Fe) as powder and the corresponding paper sheet.

The preparation of a similar sheet with the nanoMOF, yields a similar quality paper sheet, highlighting the robustness of the formulation and preparation method (Figure S5.a), the flexible character (Figure S5.b), but a slightly lower thickness of about 350 µm (Figure S5.c). All characterizations are in line with those of the previous microMOF paper sheet. The only minor differences, due to the smaller particle size, can be observed on the PXRD pattern (Figure S5.d) with, as expected, broader diffraction peaks. The main vibration modes of MIL-100(Fe) and cellulose are identified on the FTIR spectra (Figure S5.e and S5.f) while TGA (Figure S5.g) of a nanoMOF content of about 72 wt % shows the same degradation steps as the microMOF based composite. In addition, the porosity of the composite (Figure S5.h) is also in very good agreement with the nanoMOF content, with a BET specific surface area of 1245 ± 18 $m^2.g^{-1}$ vs 1720 ± 20 $m^2.g^{-1}$ for the nanoparticles. The PSD (Figure S5.i) obtained by DFT calculations remains on the whole very closed with 11.8, 17.2 and 21.4 Å pore diameters.

2.2. Impact of the MOF content

To assess the influence of the MOF content over the paper sheet properties, we first kept the same S to NFC ratio 25:75 and tuned the MOF relative ratio between 60 and 90 wt %. NanoMOF was chosen due its easy production at larger scale under ambient conditions [58]. TGA indicates an average MOF loading of 61, 72 and 90 wt %, respectively (Figure S6) and the porosity of the composites (Figure S7) is once again well correlated with the amount of loaded MOF, ranging from S_{BET} of 1090 ± 15, 1245 ± 17 to 1550 ± 20 $m^2.g^{-1}$, respectively (Table S2), with little PSD differences compared to the nanoMOF (Figure S8). In order to assess the impact of the MOF ratio on the mechanical properties of the sheet, coaxial tensile strength measurements were performed (Figure S9). The stress-strain- curves show a typical profile of paper material with an elastic region, followed by a short strain-hardening or plastic region, and finally breakage (with strain at break ranging from 0.5 to 1.5 %) [74]. Additionally, the tensile strength measurements (Figure S9) show that an increase of the MOF loading in the composite leads to a significant decrease of the tensile strength, Young modulus and a lower strain. Although the ultimate tensile strength (UTS), corresponding to the maximum stress that a material can endure when pulled before breaking, drops from 3 MPa to 1.5 MPa for the 60 wt % and the 75 wt % MOF paper sheet, respectively, both sheets can still easily be handled without creasing. However, when the loading reaches 90 wt %, the UTS of the paper sheet falls to less than 0.5 MPa, which results in a sheet too brittle for easy handling and practical use. Similarly, the strain decreases linearly with the increase of the nanoMOF loading. This confirms that the fibers content has an impact on the mechanical strength of the composite due to strengthening

role of the inter-fiber interactions. Li et al obtained better mechanical properties for TOCNF composite with 90 wt % ZIF-8 grown *in-situ* [49] or TOCNF/PEG composites loaded with 90 wt % zeolites (ZSM-5, silicalite-1 or Y) with 2 and 6-10 MPa in tensile strength, respectively [50]. However, in both cases, a considerable loss of porosity from 20 to 40 % was observed in those cases based on the BET surface areas calculations, due to a partial pore blocking and/or problem in the activation steps with possible degradation of PEG at high temperatures (T > 80 °C). In addition, both procedures [49,50] involved multi-steps, lengthy conditions or the use of hazardous solvents (DMF, methanol). The simple, ambient and green route proposed in our work enables the optimal of 75 wt % MOF loading paper that ensures sufficient mechanical stability and a high unhindered porosity thanks to the absence of pore blocking.

2.3. Optimization of the cellulosic fibers to NFC ratio

In order to further optimize the 75 wt % MIL-100(Fe) (nano or micro) paper sheets by tuning the cellulosic matrix content, the S:NFC ratio was varied as follow: 100:0, 75:25, 50:50, 25:75, 10:90 and 0:100. PXRD patterns of the resulting composites are all in good agreement with the one of the MOF (Figure S10, S11). FTIR analyses (Figure S3, S12, S13) show in all cases the main characteristic bands of MIL-100(Fe) [69] as well as those of the softwood pulp and NFC (Figures S14, S15) [72]. TGA of the paper sheets (Figure S16, S17) show that all samples are stable up to 260 °C, after which a major weight loss occurs (54-63 wt %), corresponding to a degradation of the fibers as well as the MOF's ligand. It is interesting to note that in the composites where the cellulose content is 100% S, the MOF content is lower than expected. Indeed, the micro-MOF loading in the paper sheet with 100% S is ~70 wt % and rises to ~74-78 wt % in the presence of NFC (25 % to 100 %). In the case of nano-MOF paper sheets, the same effect is observed with the MOF loading ranging from 64 wt % without NFC (100S) to ~71-73 wt % with NFC (25 to 100 %). This is probably due to a partial loss of particles during the filtration process into the filtrate and/or adhering to the filter. The MIL-100(Fe)-100S composites therefore have a more powdery aspect as shown by the residue on the adhesive tape after adhering to the sheets (Figure S18). This is in line with NFC enhancing the cohesion of the composite by acting as a microstructuring agent. Its addition enhances intermolecular bonds with MOF particles and concomitantly improves inter-fiber bonding due to the increased number of fiber-fiber interactions [39], resulting into a complex network with a better accommodation of MOF particles and the fibers. N_2 porosimetry shows, as previously, that the porosity of the composites is maintained (Figure S19-S21) with surface areas (S_{BET}) of NFC based microMOF or nanoMOF composites ranging from 1470 ± 12 to 1540 ± 13 $m^2.g^{-1}$ (Table

S3) or from 1235 ± 15 to 1245 ± 18 $m^2.g^{-1}$ (Table S4), respectively. In agreement with TGA analysis, the composites without NFC (100 % S) exhibit a lower porosity and therefore a lower BET surface area (Tables S3, S4).

In order to assess the impact of the cellulosic matrix composition as well as the MOF particle size on the mechanical properties, coaxial tensile strength measurements were performed (**Figure 3**.a, S22). The stress-strain curves evolve gradually depending on the percentage of NFC in the cellulose matrix, indicating that the ultimate tensile strength (UTS) and Young's modulus are improved by the addition of NFC in the composites made of microparticles (Figure S23) or nanoparticles (Figure S24). When containing only S, the composite is more brittle (UTS < 0.4 MPa and Young modulus < 100 MPa). However, remarkably, upon addition of a small proportion of NFC (75S:25NFC) both the UTS and related Young modulus double (with micro-MIL-100(Fe)) and even triple (nano-MIL-100(Fe)). Consequently, the paper sheet becomes less brittle and easier to handle. When the cellulose matrix contains only NFC (100NFC), the UTS reaches 1.6 MPa and 2 MPa for composites made of 75 wt % of microparticles and nanoparticles, respectively, where the bare NFC film has a UTS higher than 150 MPa [75]. Two-point bending tests were carried out to analyze the flexible character and the flexural strength of the composites (**Figure 3**.b, S25). The curves force *vs* bending angle show a linear portion, corresponding to the elastic regime up to an angle of about 20° followed by a plastic deformation (i.e. same constant force at higher angles) for the composites. One can therefore point out that a higher proportion of NFC correlates well with a higher bending force, as confirmed by the calculated bending stiffness (Figure S26). In contrast, when composites contain only NFC (100NFC), they break at a bending angle of about 20° (with very little plastic deformation) suggesting that S plays a decisive role in the flexibility of the paper sheets. Cross-sections of the 75 wt % MIL-100(Fe) loaded papers after the flexibility tests were observed with SEM (Figure S27) and showed no cracking or major differences compared to the initial samples (**Figure 2**.c, Figure S5.c). Based on these observations, a scheme is tentatively proposed to describe the synergetic effect of the two types of cellulosic fibers to form high MOF loading paper sheets with enhanced mechanical properties (**Figure 3**.c). The best compromise between flexibility and tensile strength of the paper sheets is obtained with the ratio S:NFC=25:75 (**Figure 3**) and corresponds to the folded 75 wt % MIL-100(Fe) paper sheets shown in **Figure 2**.b, S5.b. This cellulosic materials proportion was thus selected for further experiments.

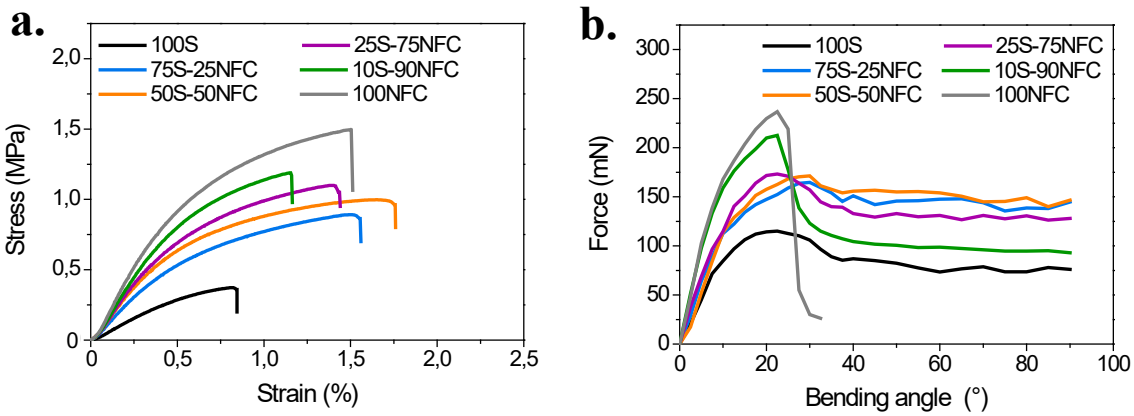

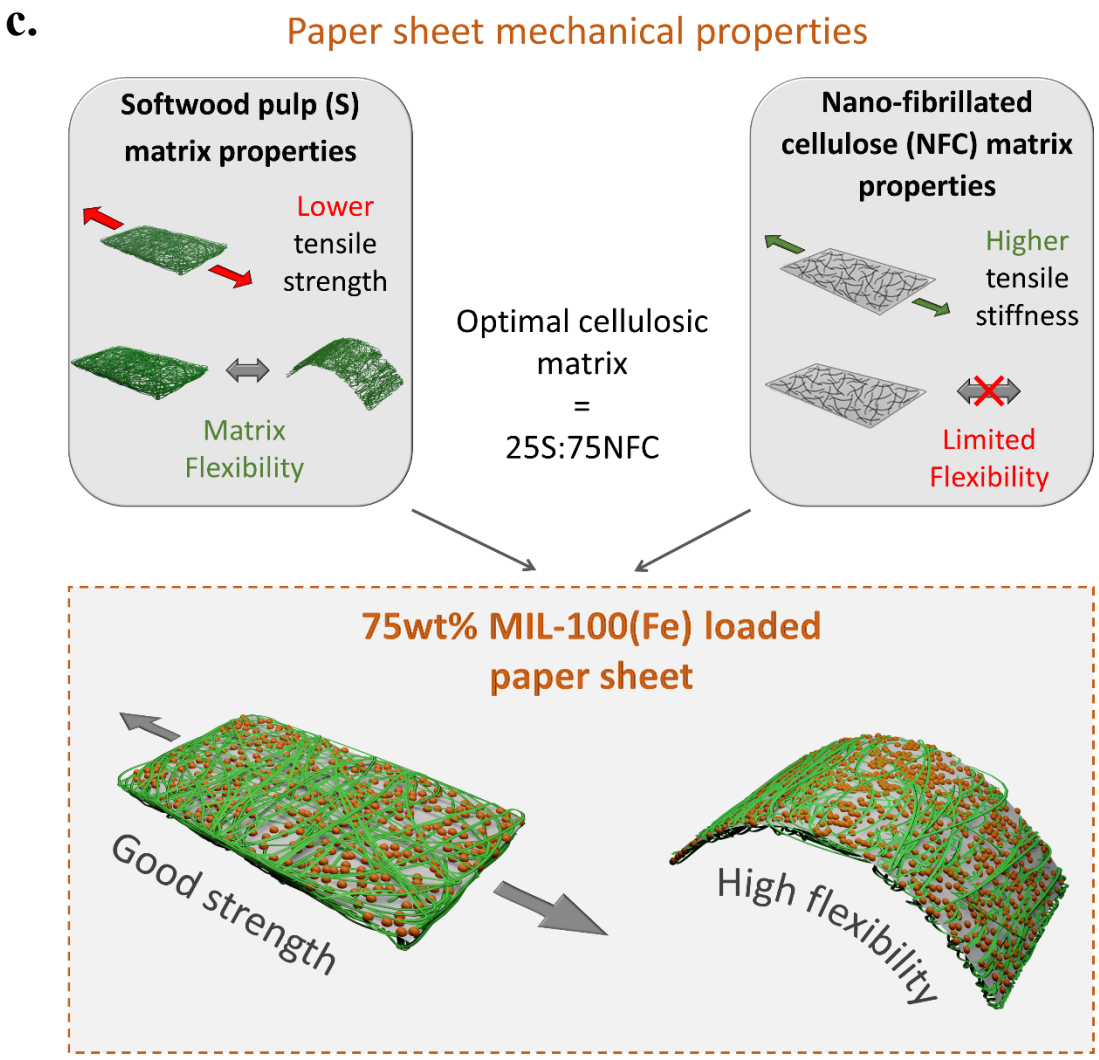

Figure 3. a) Strain-stress curves of 75 wt % micro-MIL-100(Fe) paper sheets made with different cellulosic matrices. b) Force vs angular deflection of the paper sheets containing different cellulosic matrix investigated by two-point method to deduce the flexibility of the 75 wt % micro-MIL-100(Fe) paper sheets. c) Scheme highlighting the benefits of combining two different cellulosic matrices to produce a paper sheet consisting of 75 wt % MIL-100(Fe) with good mechanical properties.

The paper sheets were then observed with an optical microscope (Figure S28, S29). The surface looks slightly irregular with a dense structure and with some identifiable fibers on the back side of the composite of several hundred microns up to a few millimeters corresponding to S fibers (Figure S30). Such an observation was confirmed by SEM which shows few particles aggregated on the surface of the paper sheet (**Figure 4**.a, S31.a, S32.a-b) and on the S fibres (Figure S31.b) with a homogeneous distribution of MOF particles on the surface and throughout the cross-section, as evidenced by Fe elemental mapping (**Figure 4**.a-d, S32.b-e). At higher magnification (**Figure 4**.e, S32.f-g), the NFC is clearly visible. It appears in the form of fibers of a few microns in length, dispersed with no preferential orientation. On the other hand, the MIL-100(Fe) microparticles are individually identifiable with an average size estimated at 1.5 ± 0.4 µm (**Figure 4**.f). The microstructure of the paper sheet was further studied using 3D X-ray microscopy by computed tomography scan (CT scan) to obtain a better view of the spatial distribution of the microMOF particles in the cellulosic matrix. The microMOF particles are homogeneously distributed in the volume (**Figure 4**.g) with some very small aggregates (tens of microns) (Figure S33.a). A cross-sectional view of the sample (Figure S33.b) shows homogeneously dispersed fibers and microMOF particles throughout the thickness (grey/white shading) with voids (black background) suggesting a macroporosity in the sample which may favour gas diffusion (bulk density = 0.275 $g.cm^{-3}$). Finally, a reconstructed 3D model (**Figure 4**.g) shows the spatial organization of the cellulosic matrix and microMOF particles throughout the volume, confirming the dense packing structure of the sheet as observed by SEM (**Figure 4**.c-d). Two short movies depicting the 3D structure observed by the CT scanner are available in the supporting information. If no filtering is applied for the low-density materials, the MOF particles and NFC can be observed as small dots while S is observed as long fibers, when moving the cutting plane through the sample (Movie 1 named MicroMIL100-full; SI). In the nano-MOF based sheets, the nanoparticles are aggregated, with an average size of 220 ± 60 nm due to the limited colloidal stability of the nano-MOF (Figure S32.h) confirmed through dynamic light scattering (DLS) where the hydrodynamic radius (aggregates surrounded by a diffuse layer) in aqueous solution is 570 nm ± 140 (at a concentration of 0.1 $g.L^{-1}$). The CT scan reveals that in this case the high-density particles are not observed as discrete particles but rather aggregated on the fibers' surface (Movie 2 named NanoMIL100; SI). Before filtration, the pH of the suspension containing the fibers/particles mixture is very acidic probably due to the partial deprotonation of trimesic carboxylic acids (pK_as = 3.16, 3.98 and 4.85) on the surface of the particles (pH=2,5 for the nanoparticles and 3,5 for the microparticles, respectively) [76]. Zeta potential measurements of the individual components were carried over the pH range 2.5-

6.5 (Figure S34). Up to about pH 3.5, MIL-100(Fe) particles are positively charged and become negatively charged above this pH. NFC being negatively charged over the whole pH range due to possible residual cellulose and hemicellulose carboxyls [70], a pH below 3.5 may enhance the electrostatic attraction between the NFC and the MOF particles.

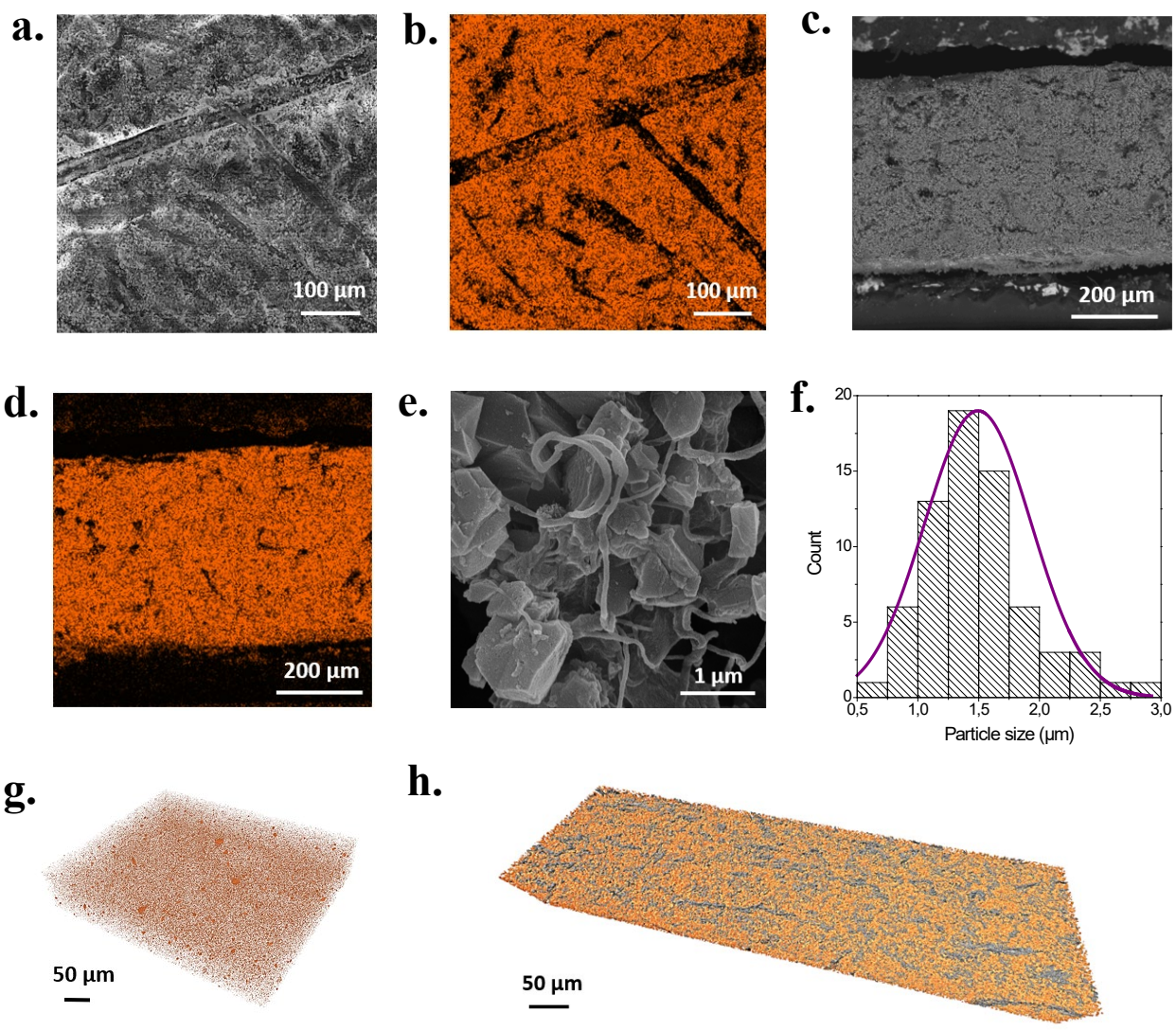

Figure 4. a-d) SEM observation of the paper with a-b. flat (scale bar = 100 µm) and c-d. cross-section (scale bar = 200 µm). b) and d) are the EDX elemental maps of iron (Fe) in the 75 wt % micro-MIL-100(Fe) paper sheet 25S-75NFC: e) SEM image of the paper sheet at higher magnification (x151000, scale bar = 1 µm). f) Histogram showing the particle size distribution of micro-MIL-100(Fe) in the paper sheet using Image J software (scale bar = 50µm). g-h) CT scan images 75 wt % micro-MIL-100(Fe) paper sheet: d. 3D reconstruction of micro-MIL-100(Fe) particles into a defined volume (scale bar = 50µm), h. 3D model of the paper sheet (cellulosic matrix in grey and micro-MOF in orange) base on the CT scanning data.

However, cellulose is known to degrade when in contact with acids [77,78]. This is due to the acid-catalyzed hydrolysis reaction which cleaves the glycosidic bonds in cellulose and hence

leads to a decrease in the degree of polymerization (DP) [79], which in turn leads to a decrease in the mechanical properties of paper [78,80]. In addition, both the MOF particles and the cellulosic fibers exhibit a specific charge – pH behavior that might impact the overall stability of the sheet: at pH 6 both NFC fibers and MOF particles have a negative surface charge causing possible electrostatic repulsions (Figure S34). To better characterize this, the impact of the pH of the suspension MOF/cellulose on the mechanical properties of the composite was studied. This also helped shedding light on the possible interactions within the composite between the fibers and the MOF particles. The pH of nano and micro MOF suspensions was first increased to pH 6 by adding a few drops of diluted aqueous NaOH solution (C = 10^{-3} M) prior to adding the MOF particles to form 75 wt % MIL-100(Fe) composite (cellulosic matrix S:NFC=25:75). Nitrogen porosimetry carried out before and after the pH adjustment at 77 K indicated no significant differences between the composites (*i.e*. same porosity) (Figure S35, S36, Table S5). Tensile strength measurements (Figure S37.a) were performed and showed a slight improvement of the UTS and Young's modulus for micro- and nanocomposites prepared at pH 6 in comparison with the sheets prepared under more acidic conditions (Figure S37.b-d). The flexural behavior was assessed and showed that the flexural stiffness was improved to a similar level for the micro- and nano-scale MIL-100(Fe) paper sheets prepared at pH 6 (Figure S38). The acid-catalysed degradation of cellulose follows first order kinetics (random reaction). The decrease of DP versus time is generally steeper at the beginning and then it reaches the "levelling-off" degree of polymerization (LODP) (where hydrolysis continues at a much slower rate) [78,81]. Gurnagul et al. investigated the relationship between DP and tensile strength by exposing kraft pulp handsheets to a hydrochloric acid solution (C = 2.6 M) at 45 °C during unspecified periods of time [80]. The DP varied from an initial value of 1600 to about 1300, a 20 % drop and the zero-span tensile strength dropped linearly by 50 %. This indicates that when in suspension in an acidic pH solution, the DP, and hence the mechanical properties of the composite, can be significantly impacted by the fibers' degradation. However, compared to their conditions, the suspension was less acidic, the temperature was lower (room temperature) and presumably the contact time shorter. Despite the change in surface charges at pH 6 (promoting electrostatic repulsions), the composites exhibit better mechanical properties than those prepared from suspensions at acidic pH. This indicates that the electrostatic interactions play a minor role in the mechanical properties of the composite and that, as in paper, the dominant forces are more likely to be hydrogen bonds between fibers.

2.4. Application to other porous solids

As the strategy was initially optimized using the benchmark MOF MIL-100(Fe), it was interesting to assess whether the methodology could be generalized to other adsorbents with different structural and chemical features (pore size, composition, particle aspect ratio). For the preparation of 75 wt % porous solids composites relying on a cellulose matrix with a 25S-75NFC ratio, we selected hydrophobic adsorbents such as MIL-53(Al)-CF_3, a microporous perfluorinated Al 1,4-benzenedicarboxylate MOF synthetized in water under reflux (more details given in the experimental section) of interest for the capture of polar VOCs [82] (Figure S39), and activated carbon, a commercial adsorbent (Figure S40), as well as the hydrophilic zeolite NaY (Figure S41). The particles size and shape depend on the nature of the adsorbent (**Figure 5.a-f**). In the case of MIL-53(Al)-CF_3, the rod-like particles are relatively monodispersed and aggregated with an average size of 190 ± 50 nm while for NaY consists of larger octahedral particles of 700 ± 115 nm. Activated carbon is more polydisperse with randomly shaped particles ranging from a few microns to almost 100 microns. A similar preparation method as for the MIL-100(Fe) sheets was followed in all cases. Remarkably, all sheets are visually smooth and homogeneous (Figure S42, S43) with good flexibility (**Figure 5.g-i**). All characterizations (PXRD, FTIR, TGA, N_2 adsorption/desorption) showed no impact on the structural and adsorption properties of the adsorbents (Figure S39-41, **Table 1**). Even if a case-by-case optimization would be needed for each sorbent, in a preliminary approach, this demonstrates that the simple preparation route developed enables the one-pot, rapid, green production of high-quality paper sheets with good mechanical properties with a large range of porous solids. Note that all these paper sheets (Figure S44) are stable in water, with no defibrillation or particle shedding.

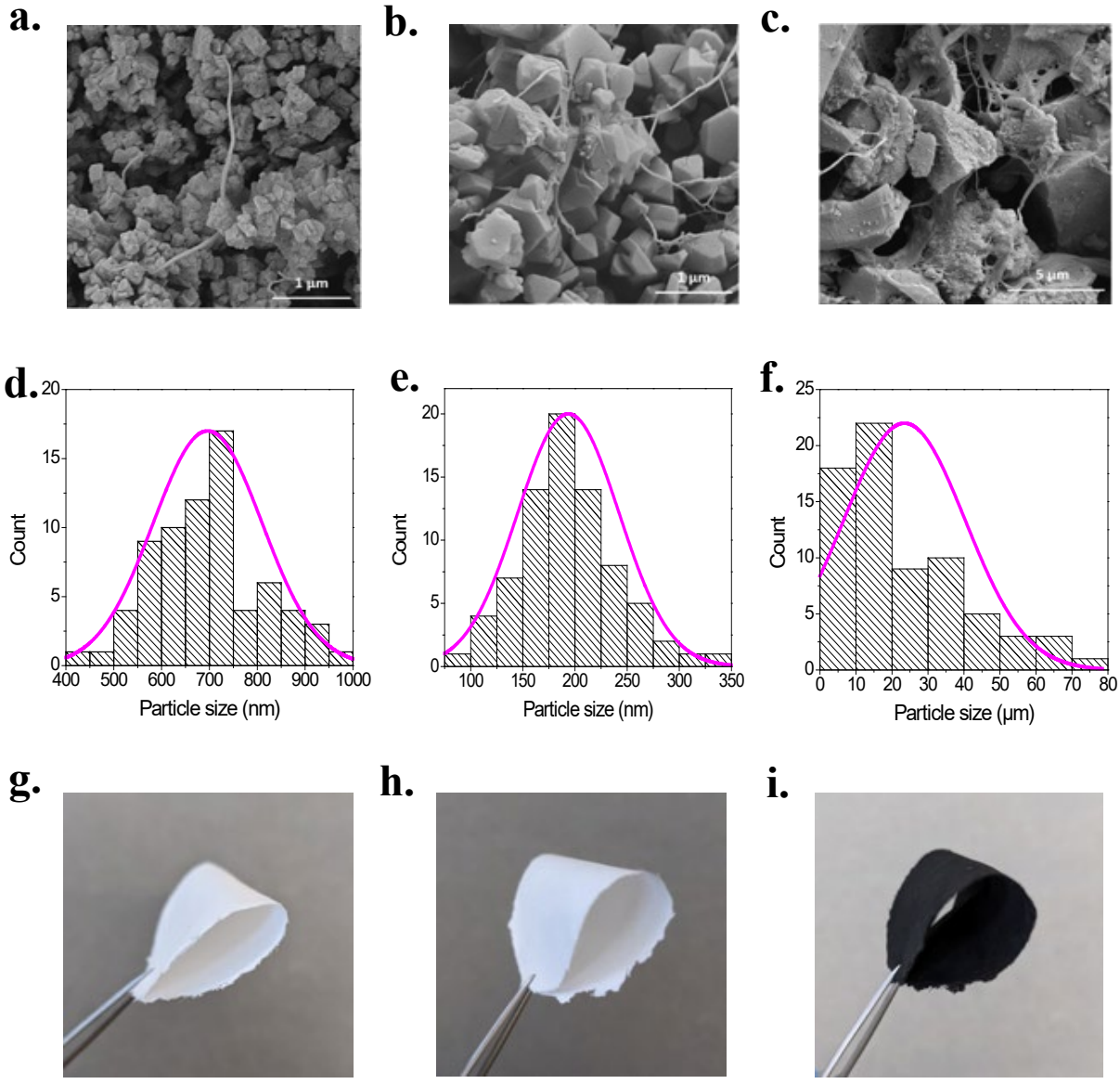

Figure 5. 75 wt % paper sheets SEM pictures (at different magnification) made with: a) MIL-53(Al)-CF_3 (x34300, scale bar = 1 µm), b) Zeolite NaY (x34300, scale bar = 1 µm) and c) Activated carbon (x8380, scale bar = 5 µm). Histograms representing the particle size distribution of: d) MIL-53(Al)-CF_3, e) Zeolite NaY and f) Activated carbon in the paper sheets using Image J software. Images showing the flexibility of the 75 wt% paper sheets made with: g) MIL-53(Al)-CF_3, h) Zeolite NaY and i) Activated carbon.

Sample	S_{BET} ($m^2.g^{-1}$)	V_{pore} ($cm^3.g^{-1}$)
MIL-53(Al)-CF_3	765 ± 3	0.35
MIL-53(Al)-CF_3 paper	565 ± 2	0.27
Zeolite NaY	860 ± 2	0.32
Zeolite NaY paper	620 ± 1	0.23
Activated carbon	1500 ± 2	1.18
Activated carbon paper	1150 ± 2	0.88

Table 1. Textural parameters of different porous solids as powder and the corresponding 75 wt % paper sheets.

2.5. Capture of Volatile Organic Compounds (VOCs)

As a preliminary attempt to assess the adsorption performances of the paper sheet, we selected acetic acid (AcOH) as a representative example of polar VOC that is challenging to capture using adsorbents due to the strong competitive adsorption with water. It has been recently demonstrated that MOFs bearing open metal(III) sites (OMS) such as MIL-100(Fe) are capable to selectively capture AcOH even in the presence of humidity through a chemisorption mechanism involving their Lewis acid sites [57]. This is of interest to museums, libraries and archives, to better preserve heritage objects that are sensitive to acid vapors (metal, ceramic, limestone, glass, among others) as well as emissive objects such as cellulose acetate-based artefacts by protecting them from auto-catalytic degradation, the so-called vinegar syndrome [83]. Shaping the MOFs being a prerequisite for these applications, we considered the use of our new MOF paper sheet to comply all the specifications.

The optimized 75 wt % micro-scale MIL-100(Fe) paper sheet was selected and its properties for the capture of acetic acid (AcOH) determined. A purpose-made set-up was used to carry out the tests using a photoionisation detector (PID) connected to a humid air (35-50 % relative humidity) test chamber (V = 0.5 dm^3) where AcOH (1 µL) was injected, corresponding to AcOH partial pressure P/P_0 of about 0.027 in the chamber. The scheme of the setup and the associated operating process as well as the method to calculate the partial pressure are described in Figure S45. The AcOH concentrations detected during a blank test with no paper sheet yielded a maximal concentration in the chamber comprised between 480 and 560 ppm (Figure S46.a). A similar experiment (Figure S46.b) was performed in the presence of the MOF paper sheet (m = 50 mg) (residence time of 30 min corresponding to the contact time between the

adsorbent and the AcOH vapors in the chamber). The AcOH concentration decreased drastically with the sheet adsorbing 95.6 ± 0.7 % of the injected AcOH. In order to discriminate the capture ability of the MOF from those of cellulose, a cellulosic sheet without MOF was also tested (Figure S46.c) (m = 12.5 mg). The fibers adsorbed only 16.5 ± 3.9 % of the 1 µL (Figure S41.d). These results demonstrate clearly that the MOF particles play the main role in the capture of AcOH within the composite. The exposure time of the MIL-100(Fe) sheet (m = 50 mg) in the chamber after AcOH injection was further extended to 90 minutes to evaluate the time necessary for the full capture of the vapors. Starting from 60 minutes onwards, 100 % of AcOH is adsorbed, suggesting that the sheet is fast adsorbing and most likely not saturated. In order to determine the saturation threshold, a constant time of 90 minutes exposure was chosen and the mass of sheet inserted into the chamber was decreased to 3.5 mg (more details given Figure S45). The AcOH concentrations detected in the chamber were the same after 90 min and one night incubation, confirming that the maximum level of adsorption of the paper sheet was reached with no change in the MOF/fibre microstructure as observed by SEM (Figure S47) and a negligible impact on the mechanical properties (Figure S48). The adsorption capacity is approximately 4.1 mmol AcOH per gram of paper sheet, similar to that obtained with nano-MOF (4 $mmol_{AcOH}.g^{-1}_{paper}$). The higher the MOF loading of the paper, the greater the AcOH adsorption capacity, increasing from 3.3 to 4.8 $mmol_{AcOH}.g^{-1}_{paper}$ for 60 and 90 wt % nano-MIL-100(Fe) loaded papers, respectively (Figure S49). Note that the paper sheet loaded with 75 wt % micro-MIL-100(Fe) could be regenerated by a simple soaking in water at room temperature (more details given in the experimental section) after which the same adsorption capacity for AcOH was fully recovered (4.1 $mmol_{AcOH}.g^{-1}_{paper}$, Figure S50).

In order to better evaluate the impact of MOF shaping on the adsorption properties, the AcOH adsorption isotherm of the 75 wt % MIL-100(Fe) loaded paper sheet was compared to the ones of the traditional MOF beads containing 85-95 wt % of MIL-100(Fe) made by wet granulation using different inorganic or organic binders (characterizations in Figure S51). Noteworthy, at a P/P_0 below 0.05, that corresponds to the binding of the AA on the open metal sites, the AcOH isotherms at 25°C (Figure S52) showed that the paper sheet exhibits a performance identical to the powder, while performing much better than the granules and the beads. These results confirm that the shaping as a paper sheet does not alter the physicochemical properties of the MOF, while the traditional mechanical shaping using various binders most likely is associated here with a partial poisoning of the OMS, hampering the AA capture efficiency. In a second step, the adsorption behavior of MIL-100(Fe) as powder, paper sheet and beads/granules was compared using a different environmental chamber set-up (Figure S53), that simulates the

conservation storage boxes used in the cultural heritage sector, as previously reported by Dedecker et al [84]. As shown before, the MIL-100(Fe) powder is highly efficient to reduce the concentration of AcOH from 80 ppm (injected dose) to 13 ppm after 1.5 hours of exposure (Figure S54). Remarkably, the MOF paper sheet lowered the concentration further to 7 ppm (contribution of the cellulosic matrix), while the beads and granules were much less effective, with AcOH concentrations between 20 and 27 ppm, in agreement with a lower accessibility of the Lewis acid sites to capture AcOH.

Finally, we assessed the impact of the shaping on the pressure drop (Figure S55); the use of binders to shape porous solids is a well-known strategy to enhance the gas diffusivity and it is common that excessive pore blocking or lack of interparticular meso or macroporosity hamper their practical use if the pressure drop is too excessive. Here, remarkably, our MOF paper sheet exhibits a minimal pressure in comparison with a commercial paper filter, indicating that the high degree of macropores in the paper sheet is beneficial for a fast diffusion of gas species.

All these results confirm the excellent ability of the MOF paper sheet to capture acetic acid under real ambient conditions, outperforming classical mechanically shaped composites. This, associated with the easy handling, high mechanical resistance and low pressure drop of the sheet holds great promise for the use of the high porous solids loading sheets as adsorbent for applications of the removal of diverse classes of pollutants.

3. Conclusion

In this work, we developed a straightforward, rapid, scalable and versatile route for the preparation of high content porous solids paper sheets (> 70 wt %). This new preparation route in water at room temperature involved a combination of two cellulose fibers with an order of magnitude size difference, i.e. softwood bleached kraft pulp fibers that provide flexibility to the composite and NFC nanofibers with high tensile strength that act as microstructuring material, confer mechanical reinforcement and retain the smallest sorbent particles. This synergistic effect of the two cellulose-based materials led to mechanically stable composite paper sheets with, for the first time, very high adsorbent loading of 75 wt % without compromising their intrinsic adsorption properties, even outperforming those of traditional shaped particles such as beads. Noteworthy not only this method does not require any particle size control for the adsorbent (nano or micro scale), but was also shown to be applicable to different classes of porous solids whatever their structural and chemical features, from MOFs, zeolites or activated carbons. Such an unprecedented, versatile, green and scalable route paves the way for the

integration of high loading porous solids paper sheets into a wide range of potential applications, from gas phase separation, heat allocation, sensing, biomedicine, among others.

4. Experimental Section

Materials: All chemicals were used without further purification. 1,3,5-benzenetricarboxylic acid, 98% (Alfa Aesar), 2-(Trifluoromethyl)-1,4-benzenedicarboxylic acid (Angene), Acetic acid glacial, 100% (Supelco), Activated charcoal (Fisher Scientific), Aluminium chloride hexahydrate, 98% (Alfa Aesar), Bentonite (Sigma-Aldrich), Ethanol absolute anhydrous (Carlo Erba reagents), Iron fine powder (Riedel-de Haën), Iron nitrate monohydrate, 98% (Sigma Aldrich), Nanofibrillated cellulose (Celova, Weidmann), Nitric acid 65% (Carlo Erba reagents), Pural (Sasol, high purity alumina with 74% Al_2O_3 and 16% MgO), Silica (Sigma-Aldrich, 30 wt % colloidal silica solution), Sodium hydroxyde pellets, 98% (Alfa Aesar), Softwood pulp (HWBK, Canson), Zeolite Y, sodium 5.1 SiO_2 :Al_2O_3 (Alfa Aesar).

MIL-100(Fe) microparticles or $Fe_3O[C_6H_3$-$(CO_2)_3]_2.OH.nH_2O$ synthesis: 3.68 g of powdered metallic iron (66 mmol) and 9.24 g of 1,3,5-benzenetricarboxylic acid or trimesic acid (44 mmol, 1,3,5-BTC) are added to a 500 mL flask, followed by 366 mL of distilled water. The solution is stirred at 500 rpm at room temperature and a volume of 2.7 mL of nitric acid is added. The flask is left under stirring for 1 week. The solid is recovered by filtration and then re-dispersed into the reaction flask with the addition of 400 mL of distilled water under stirring (500 rpm) for 1h30 in order to eliminate the trimesic acid in the pores. The solid is filtered and re-dispersed in 400 mL of absolute ethanol for a final washing during 30 minutes at 40 °C under stirring (500 rpm). Finally, the solid is filtered and dried under vacuum at room temperature.

Synthesis of MIL-100(Fe) nanoparticles or $Fe_3O[C_6H_3$-$(CO_2)_3]_2.OH.nH_2O$ synthesis: 22 g of 1,3,5-benzenetricarboxylic acid or trimesic acid (0.1 mol, 1,3,5-BTC) were added to 3.5 L of water under mechanical stirring in a 5 L reactor. Then, 64 g of iron(III) nitrate nonahydrate (0.26 mol, $Fe(NO_3)_3.9H_2O$) were introduced in the reactor. The solution turned immediately salmon-pink while becoming cloudy. The temperature was set to 70 °C and three hours later, the same amount of reactants (linker and metal salt) was added in the reactor in the same order. The solution was kept under stirring during 2 days and the product was isolated by filtration under vacuum. The solid was washed with 4 L of water and 4 L of absolute ethanol. Finally the solid was dried under vacuum at room temperature.

Synthesis of MIL-53(Al)-CF_3 nanoparticles or Al(OH)($C_6H_3CF_3C_2O_4$): 11.584 g of aluminium chloride hexahydrate (48 mmol, $AlCl_3$), 7.5 g of 2-(trifluoromethyl)-1,4-benzenedicarboxylic acid (32 mmol, 2-BDC-CF_3) and 2.56 g of sodium hydroxide (64 mmol, NaOH) were dispersed in 400 mL of water and the mixture was kept under reflux for 16h. The solid was isolated by centrifugation (10 minutes, 12000 rpm) and then redispersed in 400 mL of absolute ethanol. The solid was washed at 70 °C overnight. The white solid was again isolated by centrifugation (same conditions) and then dried at 90 °C for 3 h in the oven.

Softwood:NFC ratio adjustment in 75 wt % MIL-100(Fe) paper sheet: X g (table S6) of softwood bleached kraft pulp (S) were dispersed using a blades blender in 1 L of distilled water and then redispersed in 4 L of distilled water and stirred. Y g (Table S5) of nano-fibrillated cellulose (NFC) gel at a concentration of 3 wt% in water was added to the mixture. Then, 2.622 g of MIL-100 micro or nanoparticles (mass adjusted according to the amount of solvent contained in the pores) were placed in 250 mL of distilled water and placed in an ultrasonic bath for 15 minutes (resulting pH of micro and nano-MIL-100(Fe) solutions was respectively 3.5 and 2.5). The solution was added to the cellulosic mixture and left stirring for 15 minutes. The suspension was then filtered under vacuum using a Rapid Köthen™ handsheet former machine. The resulting 20 cm diameter paper sheet was dried under vacuum at 85 °C for 30 minutes using a dryer attached to the handsheet machine. The resulting composite contains 75 wt % of MIL-100(Fe).

Evolution of MIL-100(Fe) percentage in the paper sheet: The same protocol as above was followed but changing the percentage of MIL-100(Fe) (nanoparticles) to 60 and 90 wt % while keeping the sheet mass constant (m=3.496 g) and the cellulosic matrix ratio 25S :75NFC (table S7).

Fixing the pH of MIL-100(Fe) paper sheets: 0.218 g of softwood pulp were dispersed using a crusher in 1 L of distilled water and then redispersed in 4 L of distilled water and stirred. 0.656 g of nano-fibrillated cellulose (NFC) was added to the mixture. Then, 2.622 g of MIL-100(Fe) micro or nanoparticles (mass adjusted according to the amount of solvent contained in the pores) were placed in 250 mL of distilled water and put in an ultrasonic bath for 15 minutes. NaOH solution ($C=10^{-3}$ M) was added dropwise until reaching pH 6. The MOF suspension was mixed to the cellulosic suspension and left under stirring for 15 minutes. The suspension was then filtered under vacuum using a Rapid Köthen™ formette machine. The resulting 20 cm

diameter paper sheet was dried under vacuum at 85 °C for 30 minutes using a dryer attached to the formette machine. The resulting composite contains 75 wt % of MIL-100(Fe).

Preparation of 75 wt % paper sheets with various porous solids: 31.25 mg of softwood pulp (HWBK™, bleached kraft pulp™) was inserted into a blade mill with 30 mL of distilled water for 2 minutes. A further 30 mL was added to this suspension. The resulting fiber mixture was dispersed during 5 minutes using an ultrasound probe (it is also possible to work in a larger volume of water to eliminate this step). 93.75mg of NFC were added to the fiber suspension and the mixture was stirred for 15 minutes. 375 mg of porous solid such as MIL-53(Al)-CF_3, zeolite NaY and activated carbon particles were dispersed in an ultrasonic bath in 10 mL of distilled water (or ethanol in the case of MIL-53(Al)-CF_3) for 10 minutes. The suspension was added to the fiber suspension and kept under stirring for 15 minutes (300 rpm). The mixture was filtered under vacuum, pressed with a mold pressing machine and dried at room temperature resulting in 7 cm diameter paper sheets.

Preparation of nano-MIL-100(Fe) based mechanical shaped composites with various binders (silica, bentonite and pural): Nano-MIL-100(Fe) powder was activated at 150°C (overnight) and kept at room temperature for 2 hours before starting the shaping process.
Granules with a 85 wt % nano-MIL-100(Fe) content were prepared using a granulation process. This method involves mixing 8.5g of nanoMOF powder and 1.5g of silica (added in the form of colloidal solution containing 30 wt% water solution) in a plastic bottle and gradually adding 11.5 mL of distilled water. To ease the shaping, the bottle is rolled to form round beads that may be slightly uneven in size.
Granules with a 95 wt % MIL-100(Fe) content were prepared using an extrusion process. 9.5 g of MIL-100(Fe) and 0.5g of pural (74% of Al_2O_3 and 16% of MgO) or bentonite as binders were mixed with 12.8 mL of distilled water. A paste was formed and fed into an extruder (Multi-LAB single-screw extruder) at a speed of 20 rpm, which pushed the paste throw a 3 mm die. The granules were cut manually at approximately 5 mm length and consequently spheronized at a speed of 1500 rpm for 30 s to 1 min. The resulting granules contained 95 wt % of nano-MIL-100(Fe).

Characterizations: Crystal structure of the porous solids was carried out by powder X-ray diffraction (XRD) using a Bruker® Advance D8 diffractometer equipped with a copper source (CuKα radiation λ_{Cu}=1.5406 Å), at room temperature, in air. Transmission Infra-Red spectra

were measured with a Nicolet iS5 spectrometer in a range from 500 to 4000 cm^{-1}. Thermogravimetric analysis was performed under O_2 using a Model Mettler Toledo™ TGA/DSC2, STAR system. The samples (approximately 10 mg of each) were heated at a rate of 5 °C/minute up to 600 °C (or 700 °C when needed). N_2 adsorption-desorption isotherms were measured at 77 K with a TriStar® II apparatus using a liquid nitrogen cryogenic bath. The samples were activated under primary vacuum using a Micromeritics® degasser overnight at temperatures between 150 and 200 °C. Surface topography of the samples was performed by scanning electron microscopy using an ultra-high resolution Tescan Clara. The spatial distribution of MOF and NFC particles was carried out by 3D X-Ray microscopy using a nano-CT SkyScan 2214, Bruker® equipped with an X-Ray tube (Tungsten source) and a CCD detector system (voltage=110 kV, current=180 µA, rotation step=0.15, number of frames 2401, exposure time=2000 ms, voxel size=0.5 µm). The reconstruction of the CT was done using the NRecon software (version 2.1.0.0, Bruker) based on the Feldkamp algorithm. CTAn software (version 1.18.8.0, Bruker) was used for the 3D analysis. A region of interest (ROI) representative of the sample was selected and, the images were binarized. The objects of interest were represented in white color. The quantitative analyses of the sample were then performed through the 3D plug-in analysis. CTVox software (Bruker) (version 3.3.0, Bruker) was used for volume rendering. Zeta-potential was investigated using a Malvern Zetasizer Nano-ZS, nano-MIL-100(Fe) and NFC aqueous suspensions were prepared at 3 wt%. Mechanical properties were carried out by tensile strength measurements using an Adamel Lhomargy® tensile machine (DY20-N™, 100 dN load cell). Each sample had a length of 10 cm and a width of 1.5 cm. The distance between the jaws was 5 cm with an elongation rate of 50 $mm.min^{-1}$ and a breakage detection set at 3%. The samples were preconditioned for at least 24 hours at 25 °C and 50% relative humidity and the tests were carried out under the same conditions. The measurement was repeated on 5 samples each. The flexibility of the paper sheets was studied using a two-point bending resistance tester (Büchel Van Der Korput). Each sample had a length of 5 cm and a breadth of 3.8 cm. The samples were preconditioned at least one day at 23 °C and 50% relative humidity and the tests were carried out under the same conditions. The measurement was repeated on 3 samples each. All bending stiffness calculations were performed according to ISO5628:2019.

Volatile organic compound capture tests: The first set-up is described on Figure S40. Measurements were done with and without sorbent in order to assess the adsorption capacity of each paper sheet. The measurement consists of 3 steps: (1) First, the PID (ppbRAE 3000+

Honeywell) is switched on to circulate filtered air through the chamber until no volatile compound is detected. The 3 valves in the chamber are then closed. (2) A volume of 1 µL of AcOH is injected into the chamber, and left for 30 minutes for homogeneous dispersion. (3) Right after, the PID is pre-set to 0 ppm by analyzing the purified air (right part of the diagram). (4) Then the amount of AcOH in the chamber is measured with the PID. The amount of AcOH decreases throughout the measurement until reaching 0 ppm as the PID pump purges the vessel at a rate of 0.5 $L.min^{-1}$. In the presence of an adsorbent, the steps are identical but 12.5 mg of cellulosic paper or 50 mg of composite (micro-MIL-100(Fe)) is first inserted into the chamber. The area covered by the VOC concentration vs. time curve during the purge represents the amount of AcOH present in the vessel. In order to compare the performance of the composites at saturation level, the mass of composite was decreased to 3.5 mg and the incubation time was extended to 1.5 hours and one night.

These optimized experimental parameters were then used to compare the adsorption properties of paper sheets consisting of 60, 75 and 90 wt % nano-MIL-100(Fe) (m = 3.5 mg). The 75 wt % micro-MIL-100(Fe) loaded paper sheet was regenerated by soaking in distilled water for two days, changing water twice a day. The composite was then activated under vacuum at 150°C overnight. The regenerated composite (m = 3.5 mg) was tested again in the environmental chamber with an exposure time of 1.5 hours.

AcOH adsorption isotherms of MIL-100(Fe) powder, MIL-100(Fe) paper (75 wt % loading) and MIL-100(Fe) beads and granules (85 - 95 wt % loading) were carried out using a microbalance (CI Electronics) equipped with a pressure sensor (capacitance manometer MKS a-BARATRON, 10 Torrrange) at a controlled temperature of 25°C (VMR, VWB2 series, 0.2°C temperature stability). AcOH isotherms were produced by evaporating AcOH in the microbalance after purification by freeze-vacuum-thaw cycles inside a vacuum cell. The increase in mass was monitored as a function of time. When equilibrium was reached, the corresponding mass and pressure were recorded.

The second set-up is described on Figure S44. Measurements were performed with MIL-100(Fe) as powder and MIL-100(Fe) shaped as paper sheet (75 wt% loading) or as granules (85-95 wt% loading) with different binders (silica, bentonite or pural). A test consists of inserting 50 mg of adsorbent (activated overnight at 150°C) into the environmental chamber at a relative humidity of 40% controlled using a saturated potassium carbonate solution to obtain a stream of nitrogen with moisture. Before starting the measurement, the chamber was flushed with nitrogen and moisturefor 1.5 hours to create an equilibrium between the atmosphere and

the adsorbent. The nitrongen inlet and outlet is closed just before injecting 1µL of AcOH using a syringe. The concentration of AcOH was measured in real time in the chamber for 1.5 hours.

Supporting Information

Supporting Information is available from the Wiley Online Library or from the author.

Conflict of Interest

The authors declare no conflict of interest.

Acknowledgements

This work was funded by the European Union's Horizon 2020 research and innovation program under grant agreement No 760801\Nemosine, and by Fundação para a Ciência e a Tecnologia (FCT) in the scope of the projects UIDB/04028/2020 & UIDP/04028/2020 (CERENA). Our thanks to Karine Janel, Nathalie Marlin, Gérard Mortha and Jérémie Viguié from INP Grenoble, for helping us prepare the 20 cm paper sheets and perform the mechanical flexibility tests at Pagora (LGP2, UMR5518); to Stéphane Bouvet and Eléonora Pelizzi at Bibliothèque Nationale de France (BNF) for access to the tensile testing equipment; to Sabrina Paris Lacombe for help in obtaining the right conditions for the tensile strength measurements; to Georges Mouchaham for helping to draw porous solids structures on Diamond at ESPCI (IMAP, UMR8004); to Weidmann for providing free samples of NFC.

Received: ((will be filled in by the editorial staff))
Revised: ((will be filled in by the editorial staff))
Published online: ((will be filled in by the editorial staff))

References

[1] X-Y. Yang, L-H. Chen, Y. Li, J. C. Rooke, C. Sanchez, B-L. Su, *Chem. Soc. Rev.* **2017**, 46, 481.

[2] M-H. Sun, S-Z. Huang, L-H. Chen, Y. Li, X-H. Yang, Z-Y. Yuan, B-L. Su, *Chem. Soc. Rev.* **2016**, 45, 3479.

[3] M. E. Devis, *Nature.* **2002**, 417, 813-821.

[4] J. Liang, Z. Liang, R. Zou, Y. Zhao, *Adv. Mater.* **2017**, 29, 1701139.

[5] R. E. Morris, P. S. Wheatley, *Angew. Chem. Int. Ed.* **2008**, 47, 4966.

[6] R-B. Lin, S. Xiang, W. Zhou, B. Chen, *Chem.* **2020**, 6, 337.

[7] D. J. Wales, J. Grand, V. P. Ting, R. D. Burke, K. J. Edler, C. R. Bowen, S. Mintova, A. D. Burrows, *Chem. Soc. Rev.* **2015**, 44, 4290.

[8] W. Li, J. Liu, D. Zhao, *Nature Rev. Mater.* **2016**, 1, 16023.

[9] P. Horcajada, R. Gref, T. Baati, P. K. Allan, G. Maurin, P. Couvreur, G. Férey, R. E. Morris, C. Serre, *Chem. Rev.* **2012**, 112, 2, 1232.

[10] J. R. Holst, A. I. Cooper, *Adv. Mater.* **2010**, 22, 5212.

[11] U. Mueller, M. Schubert, F. Teich, H. Puetter, K. Schierle-Arndt, J. Pastré, *J. Mater. Chem.* **2006**, 16, 626.

[12] B. Valizadeh, T. N. Nguyen, K. C. Stylianou, *Polyhedron.* **2018**, 145, 1.

[13] G-P. Hao, W-C. Li, D. Qian, G-H. Wang, W-P. Zhang, T. Zhang, A-Q. Wang, F. Schüth, H-J. Bongard, A-H. Lu, *J. Am. Chem. Soc.* **2011**, 133, 29, 11378.

[14] R. Bingre, B. Louis, P. Nguyen, *Catalysts.* **2018**, 8, 163.

[15] A. Permyakova, O. Skrylnyk, E. Courbon, M. Affram, S. Wang, U-H. Lee, A. H. Valekar, F. Nouar, G. Mouchaham, T. Devic, G. De Weireld, J-S. Chang, N. Steunou, M. Frère, C. Serre, *ChemSusChem.* **2017**, 10, 1419.

[16] D. Bazer-Bachi, L. Assié, V. Lecocq, B. Harbuzaru, V. Falk, *Powder Tech.* **2014**, 255, 52.

[17] X-M. Liu, L-H. Xie, Y. Wu, *Inorg. Chem. Front.* **2020**, 7, 2840.

[18] R. Bingre, B. Louis, P. Nguyen, *Catalysts.* **2018**, 8, 163.

[19] K. Ma, K. B. Idrees, F. A. Son, R. Maldonado, M. C. Wasson, X. Zhang, X. Wang, E. Shehayeb, A. Merhi, B. R. Kaafarani, T. Islamoglu, J. H. Xin, O. K. Farha, *Chem. Mater*. **2020**, 32, 17.

[20] J. Zhao, B. Gong, W. T. Nunn, P. C. Lemaire, E. C. Stevens, F. L. Sidi, P. S. Williams, C. J. Oldham, H. J. Walls, S. D. Shepherd, M. A. Browe, G. W. Peterson, M. D. Losego, G. N. Parsons, *J. Mater. Chem. A.* **2015**, 3, 1458.

[21] H-W. Liang, X. Cao, W-J. Zhang, H-T. Lin, F. Zhou, L-F. Chen, S-H. Yu, *Adv. Funct. Mater.* **2011**, 21, 3851.

[22] Z. D. Anis, A. Khalil, Saepurahman, G. Singaravel, R. Hashaikeh, *Microporous and Mesoporous Materials.* **2016**, 236, 176.

[23] J. Chen, Z. Huang, H. Zhang, Z. Zhang, D. Wang, D. Xia, C. Yang, M. Dong, Chem. Eng. J. **2022**, 443, 136234.

[24] Y. Dou, W. Zhang, A. Kaiser, *Adv. Sci.* **2020**, 7, 1902590.

[25] M. J. Soberman, L. Wang, D. Jia, W. Xia, J. Li, Z. Guo, *Separation and Purification Technology*. **2020**, 253, 117461.

[26] Y. Zhang, S. Yuan, X. Feng, H. Li, J. Zhou, B. Wang, *J. Am. Chem. Soc.* **2020**, 138, 5785.

[27] D. Kang, H. Kang, *Applied Surface Science.* **2016**, 387, 82.

[28] J. Xiong, A. Li, Y. Liu, L. Wang, X. Qin, J. Yu, *J. Mater. Chem. A*. **2021**, 9, 37.

[29] A. Wang, R. Fan, X. Zhou, S. Hao, X. Zheng, Y. Yang, *ACS Appl. Mater. Interfaces*. **2018**, 10, 11.

[30] Y. Chen, S. Li, X. Pei, J. Zhou, X. Feng, S. Zhang, Y. Cheng, H. Li, R. Han, B. Wang, *Angew. Chem. Int. Ed.* **2016**, 55, 10.

[31] K. Ma, T. Islamoglu, Z. Chen, P. Li, M. C. Wasson, Y. Chen, Y. Wang, G. W. Peterson, J. H. Xin, O. K. Farha. *J. Am. Chem. Soc.* **2019**, 141, 39, 15626.

[32] D. Klemm, B. Heublein, H-P. Fink, A. Bohn, *Angew. Chem. Int. Ed.* **2015**, 54, 9029.

[33] H. Cheng, L. Li, B. Wang, X. Feng, Z. Mao, G. J. Vancso, X. Sui, *Progress in Polym. Sci.* **2020**, 106, 101253.

[34] X-F. Zhang, Z. Wang, M. Ding, Y. Feng, J. Yao, *J. Mater. Chem. A.* **2021**, 9, 23353.

[35] H. N. Abdelhamid, A. P. Mathew, *Coordination Chemistry Reviews.* **2022**, 451, 214263.

[36] P. Küsgens, S. Siegle, S. Kaskel, Adv. Eng. Mater. **2009**, 11, 1.

[37] B. Zhang, H. Chen, Q. Hu, L. Jiang, Y. Shen, D. Zhao, Z. Zhou, Adv. Funct. Mater. **2021**, 31, 2105395.

[38] S. Mintova, V. Valchev, *Zeolites.* **1995**, 16, 31.

[39] M. A. Hubbe, R. A. Gill, *BioResources.* **2016**, 11, 1, 2886.

[40] H. Katsuzawa, N. Kinoshita, H. Shouji, M. Odagiri, H. Zhang, *J. Fiber Soc. Japan.* **1994**, 50, 452.

[41] B. Thomas, M. C. Raj, K. B. Athira, M. H. Rubiyah, J. Joy, A. Moores, G. L. Drisko, C. Sanchez, *Chem. Rev.* **2018**, 118, 11575.

[42] R. J. Moon, A. Martini, J. Nairn, J. Simonsen, J. Youngblood, Chem. Soc. Rev. **2011**, 40, 3941.

[43] B. D. Mattos, B. L. Tarely, L. G. Greca, T. Kämäräinen, W. Xiang, O. Cusula. W. L. E. Magahaes, O. J. Rojas, *Sci. Adv*. **2020**, 6, 19.

[44] D. Klemm, F. Kramer, S. Moritz, T. Lindström, M. Ankerfors, D. Gray, A. Dorris, *Angew. Chem. Int. Ed.* **2011**, 50, 5438.

[45] A. Sobhan, K. Muthukumarappan, Z. Cen, L. Wei, *Carbohydrate Polym*. **2019**, 225, 115189.

[46] Z. Wang, M. Li, X-F. Zhang, Y. Zhou, J. Yao, *Cellulose.* **2022**, 29, 1873.

[47] Z. Zhang, N. Ma, S. Yao, W. Han, X. Li, H. Chang, Y-Y. Wang, *ACS Sustainable Chem. Eng.* **2021**, 9, 5827.

[48] M. Matsumoto, T. Kitaoka, *Adv. Mater.* **2016**, 28, 1765.

[49] S-C. Li, B-C. Hu, L-M. Shang, T. Ma, C. Li, H-W. Liang, S-H. Yu, Adv. Mater. **2022**, 34, 2202504.

[50] N. Keshavarzi, F. Mashayekhy Rad, A. Mace, F. Ansari, F. Akhtar, U. Nilsson, L. Berglund, L. Bergström, *ACS Appl. Mater. Inter.* **2015**, 7, 14254.

[51] A. J. Svagan, M. A. S. Azizi Samir, L. A. Berglund, *Adv. Mater.* **2008**, 20, 1263.

[52] S. K. Bismas, H. Sano, M. I. Shams, H. Yano, *ACS Appl. Mater. Inter.* **2017**, 9, 35, 30177.

[53] M. F. F. Pego, M. L. Bianchi, P. K. Yasumura*, Wood Science and Technology.* **2020**, 54, 1587.

[54] G. Fathi, J. E. Kasmani, *BioResources.* **2019**, 14, 2.

[55] P. Horcajada, S. Surblé, C. Serre, D-Y. Hong, Y-K. Seo, J-S. Chang, J-M. Grenèche, I. Margiolaki, G. Férey, *Chem. Commun.* **2007**, 2820.

[56] S. Wuttke, A. Zimpel, T. Bein, S. Braig, K. Stoiber, A. Vollmar, D. Vollmar, D. Müller, K. Haastert-Talini, J. Schaeske, M. Stiesch, G. Zahn, A. Mohmeyer, P. Behrens, O. Eickelberg, D. A. Bölükbas, S. Meiners, *Adv. Healthcare Mater.* **2017**, 6, 1600818.

[57] M. I. Severino, A. Al Mohtar, C. V. Soares, C. Freitas, N. Sadovnik, S. Nandi, G. Mouchaham, V. Pimenta, F. Nouar, M. Daturi, G. Maurin, M. L. Pinto, C. Serre, *Angew. Chem. Int. Ed.* **2023**, 62, e202211583.

[58] A. Permyakova, S. Wang, E. Courbon, F. Nouar, N. Heymans, P. D'Ans, N. Barrier, P. Billemont, G. De Weireld, N. Steunou, M. Frère, C. Serre, *J. Mater. Chem. A.* **2017**, 5, 12889.

[59] Y-K. Seo, J. W. Yoon, J. S. Lee, Y. K. Hwang, C-H. Jun, J-S. Chang, S. Wuttke, P. Bazin, A. Vimont, M. Daturi, S. Bourrelly, P. L. Llewellyn, P. Horcajada, C. Serre, G. Férey, *Adv. Mater.* **2012**, 24, 806.

[60] M. Tong, D. Liu, Q. Yang, S. Devautour-Vinot, G. Maurin, C. Zhong, *J. Mater. Chem. A.* **2013**, 1, 8534.

[61] G. Gnanasekaran, A. G, T. S. Mok, *Separation and Purification Technology.* **2021**, 277, 119655.

[62] A. Dhakshinamoorthy, M. Alvaro, P. Horcajada, E. Gibson, M. Vishnuvarthan, A. Vimont, J-M. Grenèche, C. Serre, M. Daturi, H. Garcia, *ACS Catal.* **2012**, 2(10), 2060.

[63] S. Wuttke, P. Bazin, A. Vimont, C. Serre, Y-K. Seo, Y. K. Hwang, J-S. Chang, G. Férey, M. Daturi, *Chem. Eur. J.* **2012**, 18, 11959.

[64] E. Soubeyrand-Lenoir, C. Vagner, J. W. Yoon, P. Bazin, F. Ragon, Y. K. Hwang, C. Serre, J-S. Chang, P. L. Llewellyn, *J. Am. Chem. Soc.* **2012**, 134(24), 10174.

[65] J. W. Yoon, Y-K. Seo, Y. K. Hwang, J-S. Chang, H. Leclerc, S. Wuttke, P. Bazin, A. Vimont, M. Daturi, E. Bloch, A. L. Llewellyn, C. Serre, P. Horcajada, J-M. Grenèche, A. E. Rodrigues, G. Férey, *Angew. Chem. Int. Ed.* **2010**, *49*, 5949.

[66] P. Horcajada, C. Serre, M. Vallet-Regi, M. Sebban, F. Taulelle, G. Férey, *Angew. Chem. Int. Ed.* **2006**, *118*, 6120.

[67] S. Sene, M. T. Marcos-Almaraz, N. Menguy, J. Scola, J. Volatron, R. Rouland, J-M. Grenèche, S. Miraux, C. Menet, N. Guillou, F. Gazeau, C. Serre, P. Horcajada, N. Steunou, *Chem.* **2017**, *3*, 2.

[68] M. Giménez-Marqués, A. Santiago-Portillo, S. Navalon, M. Alvaro, V. Briois, F. Nouar, H. Garcia, C. Serre, *J. Mater. Chem. A.* **2019**, *7*, 20285.

[69] F. Nouar, M. Manchal, M. Benzaqui, N. Steunou, M. Gimenez-Marques, S. Sene, C. Serre. Low temperature process for the synthesis of MOF carboxylate nanoparticles. European patent application 17305119.4. **2017**.

[70] E. J. Foster, R. J. Moon, U. P. Agarwal, M. B. Bortner, J. Bras, S. Camarero-Espinosa, K. J. Chan, M. J. D. Clift, E. D. Cranston, S. J. Eichborn, D. M. Fox, W. Y. Hamad, L. Heux, B. Jean, M. Korey, W. Nieh, J. A. Shatkin, J. Simonsen, K. Stinson-Bagby, N. Wanasekara, J. Youngblood, *Chem. Soc. Rev.* **2018**, *47*, 2609.

[71] Y-K. Seo, J. W. Yoon, J. S. Lee, U-H. Lee, Y. K. Hwang, C-H. Jun, P. Horcajada, C. Serre, J-S. Chang, *Microporous and Mesoporous Mater.* **2012**, *157*, 137.

[72] E. Abraham, B. Deepa, L. A. Pothan, M. Jacob, S. Thomas, U. Cvelbar, R. Anandjiwala*, Carbohydrate Polymers.* **2011**, *86*, 1468.

[73] J. Zhao, W. Zhang, X. Zhang, X. Zhang, C. Lu, Y. Deng, *Carbohydrate Polymers.* **2013**, *97*, 695.

[74] M. Henriksson, L. A. Berglund, P. Isaksson, T. Linsdtröm, T. Nishino, *Biomacromolecules.* **2008**, *9*, 1579.

[75] E. Oliaei, P. A. Lindén, Q. Wu, F. Berthold, L. Berglund, T. Lindström, *Cellulose.* **2020**, *27*, 2325.

[76] E. Bellido, M. Guillevic, T. Hidalgo, M. J. Santander-Ortega, C. Serre, P. Horcajada, *Langmuir.* **2014**, *30*, 20.

[77] O. Soubelet, M. A. Presta, M. Marx, Die Makromolekulare Chemie. **1989**, *190*, 12.

[78] T. P. Nevell. *Degradation of cellulose by acids, alkalis and mechanical means*. In Cellulose Chem and its Applications (Nevell, T. P. ed.). Ellis Horwood. **1985**.

[79] E. Kontturi, A. Meriluoto, P. A. Penttilä, N. Baccile, J-M. Malho, A. Potthast, T. Rosenau, J. Ruokolainen, R. Serimaa, J. Laine, H. Sixta, *Angew. Chem. Int. Ed.* **2016**, *55*, 14455.

[80] N. Gurnagul, D. H. Page, M. G. Paice, *Nordic Pulp and Paper Research*. **1992**, *311992*, 152.

[81] J. Tétreault, P. Bégin, S. Paris-Lacombe, A-L. Dupont, *Cellulose.* **2019**, *26*, 2013.

[82] M. I. Severino, A. AI Mohtar, C. V. Soares, O. Kolmykov, C. Freitas, I. Dovgaliuk, C. Martineau-Corcos,V. Pimenta, F. Nouar, G. Maurin, M. L. Pinto, C. Serre, *J. Mater. Chem. A*. **2023**, *11*, 4238.

[83] J. Kammer, F. Truong, C. Boissard, A-L. Soulié, A-L. Dupont, L. Simon, V. Gros, B. Lavédrine. *J. Cultural Heritage*. **2021**, 47, 50.

[84] K. Dedecker, R. S. Pillai, F. Nouar, J. Pires, N. Steunou, E. Dumas, G. Maurin, C. Serre, M. L. Pinto. *ACS Appl. Mater. Interfaces*. **2018**, 10, 16.